Journal of Nuclear Materials 396 (2010) 10–19

Contents lists available at ScienceDirect

Journal of Nuclear Materials

journal homepage: www.elsevier.com/locate/jnucmat

Analysis of tensile deformation and failure in austenitic stainless steels: Part II – Irradiation dose dependence

Jin Weon Kim [a], Thak Sang Byun [b,*]

[a] Department of Nuclear Engineering, Chosun University, 375 Seosuk-dong, Dong-gu, Gwangju 501-759, Republic of Korea
[b] Oak Ridge National Laboratory, Material Science and Technology Division, P.O. Box 2008, MS-6138, Oak Ridge, TN 37831, United States

A B S T R A C T

Irradiation effects on the stable and unstable deformation and fracture behavior of austenitic stainless steels (SSs) have been studied in detail based on the equivalent true stress versus true strain curves. An iterative finite element simulation technique was used to obtain the equivalent true stress–true strain data from experimental tensile curves. The simulation result showed that the austenitic stainless steels retained high strain hardening rate during unstable deformation even after significant irradiation. The strain hardening rate was independent of irradiation dose up to the initiation of a localized necking. Similarly, the equivalent fracture stress was nearly independent of dose before the damage (embrittlement) mechanism changed. The fracture strain and tensile fracture energy decreased with dose mostly in the low dose range <~2 dpa and reached nearly saturation values at higher doses. It was also found that the fracture properties for EC316LN SS were less sensitive to irradiation than those for 316 SS, although their uniform tensile properties showed almost the same dose dependencies. It was confirmed that the dose dependence of tensile fracture properties evaluated by the linear approximation model for nominal stress was accurate enough for practical use without elaborate calculations.

Published by Elsevier B.V.

1. Introduction

Austenitic 300 series stainless steels (SSs) generally show a good resistance to irradiation embrittlement and no significant shift of ductile to brittle transition temperature by irradiation at low temperatures below 400 °C, although they show low resistance to irradiation swelling and creep above about 400 °C [1]. Those steels therefore have been not only widely used in conventional nuclear power plants, where operation temperatures are limited below ~400 °C, but also selected for advanced reactor components such as the first wall and shield of ITER [2] and container vessel for the liquid metal target of spallation neutron source [1,3–5]. A number of studies have been conducted to clarify the change in the mechanical properties of austenitic stainless steels under intense radiation environments [1–7]. All results showed that the strength, ductility, and strain hardening capacity were significantly changed by irradiation. In particular, the irradiation hardening was often accompanied by changes in the stress–strain curve along with the appearance of yield drop and by a significant reduction in strain hardening capability [4–8]. However, most of these radiation-induced changes were observed for the uniform deformation regime only based on the engineering stress–strain curves, and consequently the radiation effect on the unstable deformation has been often ignored although in most cases its range is larger than that for uniform deformation. To understand the radiation effects on deformation and fracture phenomena in detail, therefore, it is necessary to produce full stress–strain data covering yielding, uniform deformation, unstable deformation, and final failure.

It was shown that the analysis of true stress–true strain behavior can suggest new descriptions for the irradiation effects on the strength and ductility of materials [7–9]. In particular, the irradiation effects on the plastic instability and fracture properties, which are important for the structural design and life time evaluation, can be evaluated by analyzing full true stress–true strain curves of irradiated materials including unstable deformation. Previous studies [7–12] investigated irradiation effects on the fracture stress, fracture strain, and strain hardening rate from tensile data of irradiated austenitic stainless steels using a linear approximation model. They showed that the strain hardening behavior at a given true stress level was not significantly influenced by irradiation [8–10] and that the plastic instability stress and fracture stress were dose independent [8–13]. These studies, however, assumed a linear strain hardening based on the nominal true stress and true strain relationship instead of the equivalent true stress (σ_T)–true strain(ε_T) relationship, which represents more general stress and strain response of a material and is nearly independent of specimen geometry [12]. The nominal true stress during unstable deformation, which is determined by dividing the axial load by the minimum cross-sectional area of the specimen at the neck, is higher

* Corresponding author. Tel.: +1 865 576 7738.
E-mail address: byunts@ornl.gov (T.S. Byun).

0022-3115/$ - see front matter Published by Elsevier B.V.
doi:10.1016/j.jnucmat.2009.08.009

than the equivalent stress which is required to cause plastic flow if simple tension prevailed.

This study aimed at the detailed characterization of irradiation effects on the full range of deformation including unstable deformation and final failure based on the equivalent true stress and true strain relation. In this study, thus, the full equivalent true stress–true strain curves were determined from tensile data for annealed 316 SS and EC316LN SS irradiated to various doses, using an iterative finite element simulation technique. The tensile fracture properties, i.e., equivalent fracture stress, fracture strain, and tensile fracture energy, were evaluated from the calculated true stress–true strain curves. Detailed techniques are largely the same as those used for the simulation in Part I paper [14]. Based on the results, the dose dependencies of strain hardening behavior and fracture properties were investigated.

2. Tensile data for irradiated materials

Three tensile datasets for irradiated 316 SS and EC316LN SS (IR1–IR3) obtained from earlier studies [6,8,13,15] were analyzed in this study using an iterative finite element(FE) method. The materials were irradiated to various doses and tested at room temperature (RT) or at 288 °C for 316 SS and at RT for EC316LN SS. These datasets were selected to well represent the radiation effect on the deformation and facture behaviors of the austenitic stainless steels. Tables 1 and 2 summarize the chemical composition and thermo-mechanical treatment of the test materials and the irradiation and test conditions, respectively.

Irradiations were performed at two facilities as listed in Table 2: the hydraulic tube facility of the high flux isotope reactor (HFIR) at the Oak Ridge National Laboratory for 316 SS specimens and the target area of the Los Alamos Neutron Scattering Center (LANSCE) accelerator at the Los Alamos National Laboratory for EC316LN SS specimens [8,13]. In the HFIR irradiation facility, irradiation temperatures were estimated to be in the range of 60–100 °C for the specimens tested at RT and at ~350 °C for the specimens tested at 288 °C. In the LANSCE accelerator, the specimens were irradiated at different target area locations for different irradiation doses by protons and spallation neutrons [8,13]. Irradiation temperature measured was in the range of 60–160 °C. More detailed descriptions can be found elsewhere [6,15].

Two types of small-sized flat specimens were employed for tensile tests: BES/NERI type for 316 SS and S-1 type for EC316LN SS, whose gage section dimensions are 8 mm × 1.5 mm × 0.25 mm and 5 mm × 1.2 mm × 0.25 mm, respectively. All tests were conducted in the screw-driven testing machines at quasi-static nominal strain rate of about 10^{-3} s^{-1}. Fig. 1 presents engineering stress–strain curves of the materials analyzed in the present study. This figure displays that the engineering stress–strain curves are considerably changed by irradiation: increase in strength and decrease in elongation, except for 316 SS tested at 288 °C, where radiation effect was minimal.

3. Finite element simulation

A procedure for determining equivalent true stress–true strain curve beyond the onset of necking was the same as that described in the Part I paper [14]. That is, the curve after necking was determined by iterative calculations until the numerical calculation of the load and unstable deformation corresponded well with the experimental data. Finite element model was also basically the same as that used in the Part I: three-dimensional one-eighth model that consists of 20-node solid element with reduced integration (C3D20R in ABAQUS [16]). Two different geometrical models were used depending on the specimen type (see Fig. 2). In the models, the number of elements in the width and thickness directions at the center of specimen was 18 by 5 for S-1 type and 20 by 4 for BES/NERI type, which were optimized based on the convergence tests. A geometrical imperfection in a form of locally reduced width and thickness of an amount 0.25% of their dimensions was embedded in the model to allow the initiation of necking. Since the symmetry was introduced around the longitudinal axis, the embedded imperfection in the central cross-section of the model resulted in an easier computation [17–19]. The symmetry assumption is valid until almost the end of experiment, when the local instability planes at an acute angle with respect to the longitudinal axis of the sample are formed and the specimen begins tearing. In spite that the material damage and bifurcation of specimen should be considered to accurately simulate the deformation beyond the onset of localized necking, these were not taken into account in the present model for simplicity.

In the Part I paper it was confirmed that the experimental load–displacement curves could be accurately simulated by an iterative application of finite element method. The simulated and experimental curves for irradiated stainless steels are compared in Fig. 3. The strain contour and deformation pattern at final failure were also examined for the two specimen types shown in Fig. 4. The strain distribution and deformation pattern at final failure were different from those observed at the Part I paper, which used SS-3 type specimen whose cross-section is 0.76 mm × 1.52 mm. For the S-1 and BES/NERI type specimens, local instability plane at final failure formed along an oblique plane to the cross-section of specimen regardless of irradiation dose and test temperature, even though contraction of specimen in the width direction was also observed. It is also shown that the contour of the maximum principal logarithmic strain devel-

Table 1
Materials and heat-treatments [6,14].

Data ID	Materials	Chemical compositions (wt.%)	Heat treatment
IR1	316-Annealed	Fe–17.15Cr–13.45Ni–2.34Mo–1.86Mn–0.57Si–0.024P–0.059C–0.031N–0.018S–0.1Cu–0.02Co	Annealed at 1050 °C for 30 min
IR2	EC316LN	Fe–17.45Cr–12.2Ni–2.5Mo–1.81Mn–0.39Si–0.024C–0.067N	Annealed at 950 °C for 1 h
IR3	316-Annealed	Fe–17.15Cr–13.45Ni–2.34Mo–1.86Mn–0.57Si–0.024P–0.059C–0.031N–0.018S–0.1Cu–0.02Co	Annealed at 1050 °C for 30 min

Table 2
Irradiation and test conditions [6,14].

Data ID	Materials	Irradiation facility	Dose range (dpa)	Irradiation temperature (°C)	Test temperature (°C)	Specimen type
IR1	316-Annealed	HFIR	0–0.78	60–100	20	BES/NERI
IR2	EC316LN	LANSCE	0–10.7	60–160	20	SS-1
IR3	316-Annealed	HFIR	0–0.1	~350	288	BES/NERI

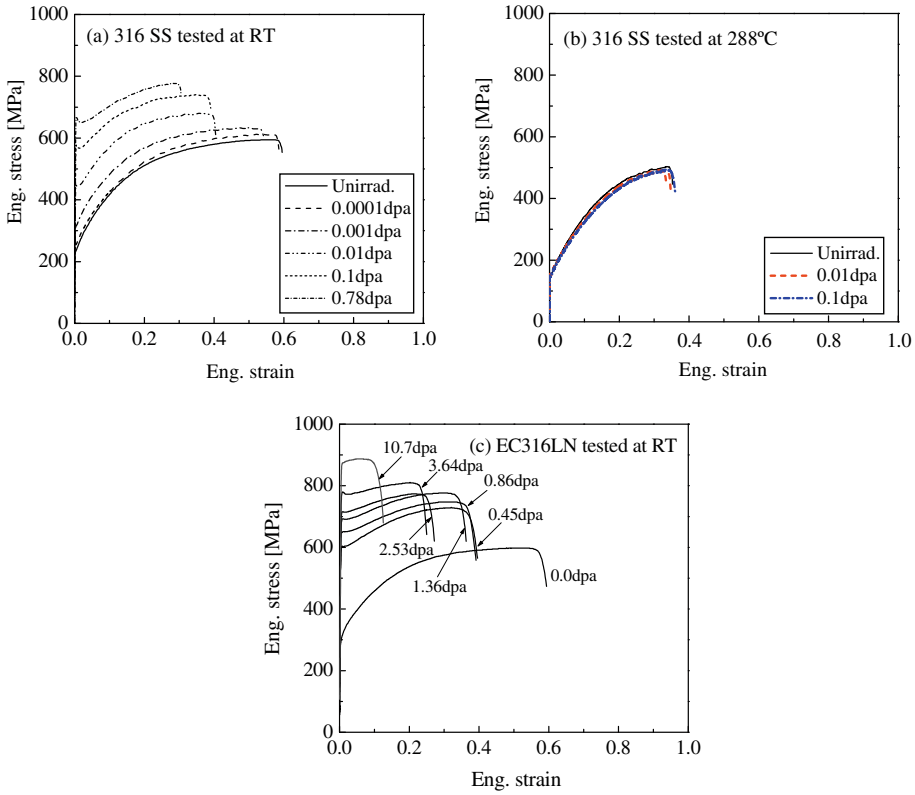

Fig. 1. Engineering stress–strain curves for irradiated austenitic stainless steels: (a) 316 SS tested at RT, (b) 316 SS at 288 °C, and EC316LN at RT [6,14].

oped along the oblique plane (see Fig. 4). These indicate that localized necking occurred along the oblique plane after initial diffuse necking and it led to the final failure of the specimens. The specific deformation characteristics are associated with the different aspect ratio of specimens: 2.0 for SS-3, 4.8 for S-1, and 6.0 for BES/NERI type specimens. It is known that the transition of necking deformation mode occurs in the aspect ratio range of 3–6 in ductile materials. The transition is believed to depend on the mechanical properties of the material as well as the initial aspect ratio of the specimen tested [19,20]. The present simulation results confirm these earlier studies: the transition from diffuse to localized necking occurred before final failure for both S-1 and BES/NERI type specimens where the aspect ratios are greater than 4.0, which is contrasted to the simulation results showing no obvious transition of necking mode in the SS-3 type specimens whose initial aspect ratio was less than 3.0.

Based on these results, it is again believed that the finite element model successfully simulates the load–displacement responses of tensile tests including the early failure process such as the localized necking. Since the microscopic damage mechanisms such as the void nucleation and growth and dislocation channeling were not taken into account in this study, the present FE simulation was not aimed at the detailed simulation of final fracture process, in particular the later part of the localized necking, and therefore the equivalent true stress–true strain curves found by simulations should be valid up to the localized necking before the final fracture process initiates. Once the localized necking started at flat specimen, the thickness along the necking band shrinks more than the width-direction contraction and the local strain increases rapidly [18,19]. A discrete, heavy deformation may occur on some slip planes within the highly localized shear band. Therefore, the strain after the onset of localized necking given by the present continuum-based simulation should be considered as a lower bound for the local strain.

4. Results and discussion

4.1. Equivalent true stress–true strain curves

Fig. 5 presents full equivalent true stress–true strain curves including unstable deformation region for 316 SS and EC316LN SS irradiated to various doses, which were determined by the iterative finite element simulations. As shown in Fig. 5a and c, the curves for RT have continuously decreasing slopes in uniform deformation region. The equivalent true stress–true strain curves did not change their slope at the onset of diffuse necking regardless of irradiation dose; the equivalent true stress still increased with true strain at similarly high rates throughout the unstable deformation before the onset of localized necking. It was also observed that the slopes of the curves varied little with irradiation dose before the significant slope change appeared at the onset of localized necking, even though the specimen at a higher dose exhibited higher equivalent true stress–true strain curve. For the 316 SS tested at 288 °C, Fig. 5b, the equivalent true stress–true strain curves were nearly the same over the whole strain range, regardless of irradiation dose. This indicates that at 288 °C the effect of irradiation on the plastic flow of 316 SS is negligible at doses below 0.1 dpa. It was also observed that at this elevated temperature the significant reduction in the slope of the curves occurs soon after the onset of necking.

In Fig. 5, the significant slope change in the equivalent true stress–true strain curves appeared after a certain amount of unstable deformation for both 316 SS and EC316LN SS tested at RT. Such a behavior was not observed for the equivalent true stress–true strain curves obtained for the SS-3 type specimens in the Part I of this paper. To understand this specific behavior, the changes of deformation pattern and strain contour with tensile loading were examined in simulation results and compared with that of equivalent true stress–true strain curve. It showed that the significant

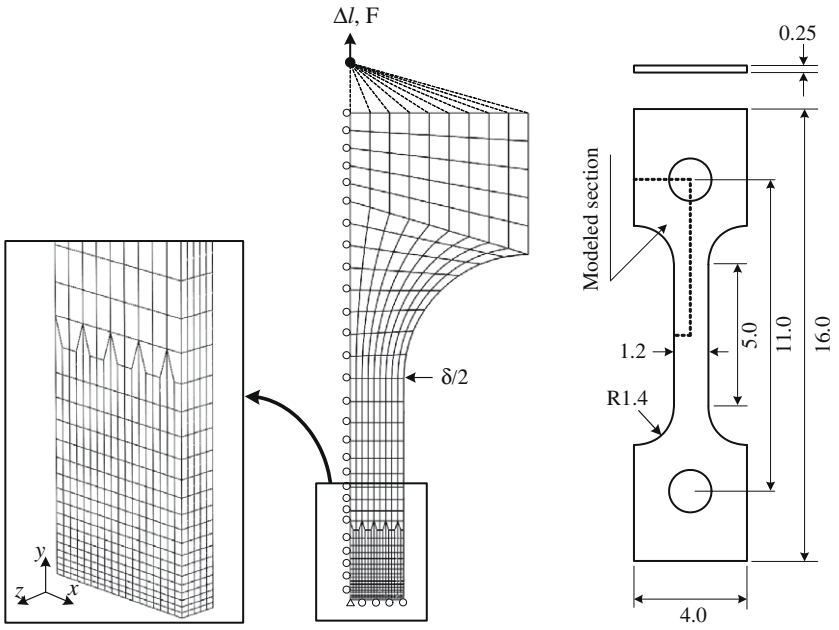

(a) S-1 type

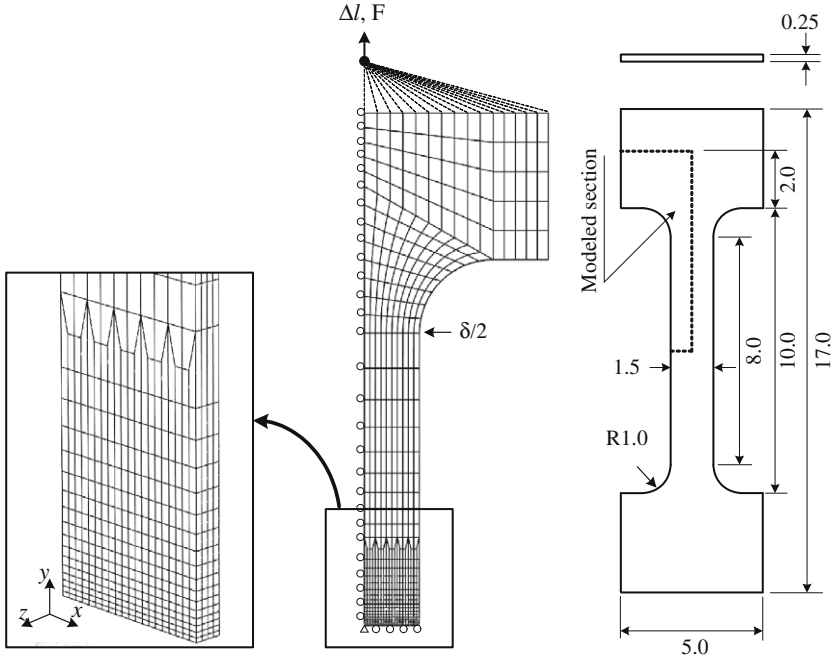

(b) BES/NERI type

Fig. 2. Finite element models for (a) the S-1 type and (b) the BES/NERI type specimens.

reduction in the slope of the curve coincides with the necking mode transition of specimen, from diffuse necking to localized necking. If the test material retains sufficient ductility in the end of diffuse necking, the transition of necking mode to localized necking occurs gradually, but over a relatively short time period when compared to the whole testing time. After a localized deformation band is formed in the diffuse neck, additional plastic deformation will be concentrated within the band and it will form a necked band before the final failure. Although the shear strain within the localized neck can be significant, its contribution to the total elongation is minimal, as indicated in the engineering stress–strain curves. Most of the strain imposed in the localized should be absorbed in the reduction of thickness. Since such concentrated straining in a narrow band may enhance dislocation annihilation, the strain hardening rate during the localized necking should be lowered from those of uniform deformation or diffuse necking.

Fig. 6 illustrates the contours of the maximum principal logarithmic stain at different deformation steps for 316 SS specimen irradiated to 0.1 dpa, which exhibited the reduction in slope at

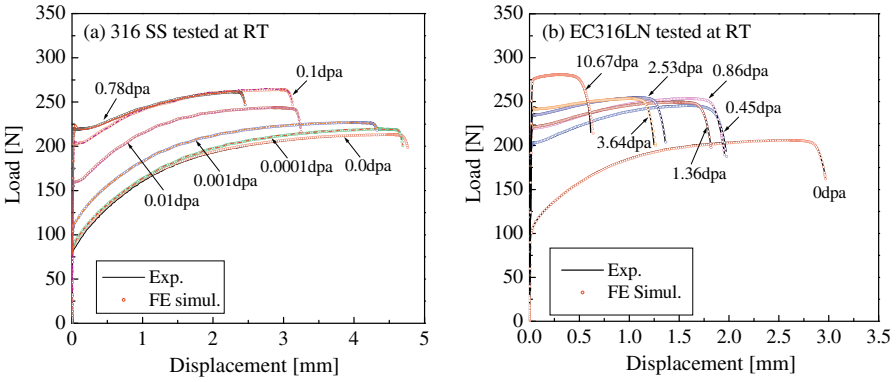

Fig. 3. Comparisons of load–displacement curves obtained from experiment and finite element simulation for (a) 316 SS and (b) EC316LN SS.

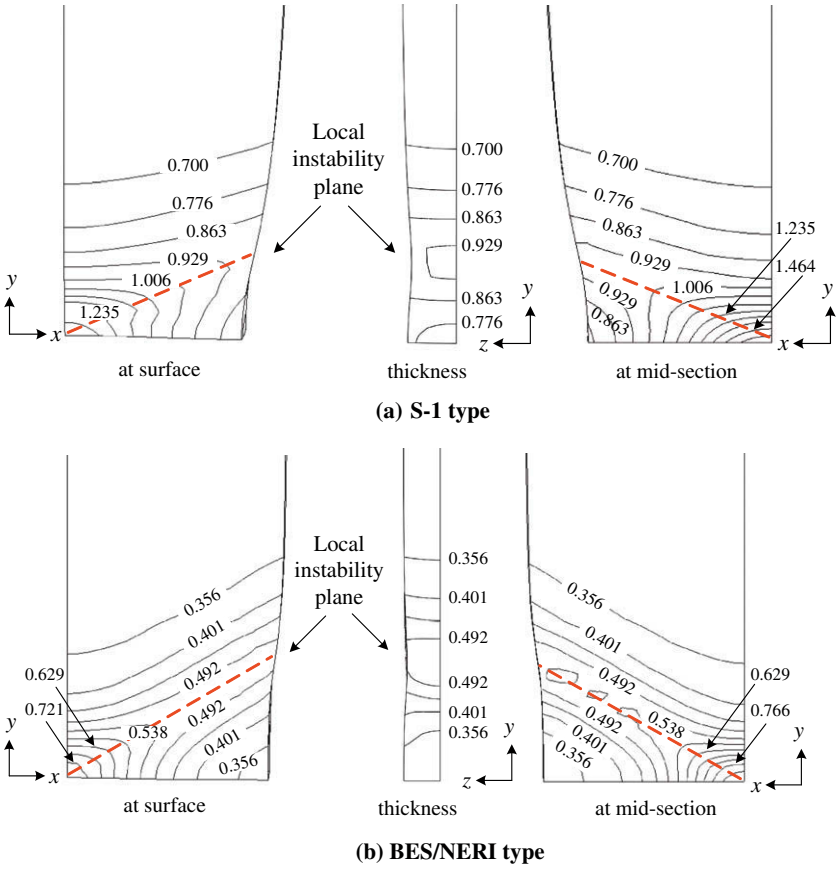

Fig. 4. Deformation patterns and maximum principal logarithmic strain distributions at final failure in (a) the S-1 type and (b) the BES/NERI type specimens.

$\varepsilon_T \approx 48\%$. A strain gradient could not be observed at $\varepsilon_T = 25\%$, the uniform strain region, and the strain contour for $\varepsilon_T = 45\%$, the diffuse necking region, propagated along the perpendicular plane to the loading axis of sample. However, at $\varepsilon_T = 50\%$ the maximum strain contour spread along an oblique plane, which is evidence of localized necking, and this pattern continued to final failure ($\varepsilon_T = 58\%$). The localized necking was assumed to initiate when the equal-strain contours obviously started to spread along an oblique plane. This transition in necking mode resulted in the reduced slopes in the equivalent true stress–true strain curves, as seen in Fig. 5. Also, this localization criterion by strain contour was compared with a stress-based criterion [11,21]:

$$\frac{d\sigma}{d\varepsilon} = \frac{\sigma}{2}. \tag{1}$$

Fig. 7 indicates that the equivalent true stress and true strain at initiation of localized necking determined from the strain contour, $\sigma_{nL,CT}$ and $\varepsilon_{nL,CT}$, are almost identical to those determined by the criterion for σ_{nL} and ε_{nL} expressed by Eq. (1).

It is shown that all the S-1 and BES/NERI specimens exhibit the necking mode transition during unstable deformation. In Fig. 5 it is seen that in the austenitic stainless steels after significant irradiation high positive strain hardening rate is still retained during unstable deformation before localized necking initiates. Further, the parallel curves indicate that the strain hardening rate is independent of irradiation dose. At 288 °C, the prompt reduction in strain hardening rate after necking is also explained by early initiation of localized necking. As discussed in the Part I of this paper, the dominant deformation mode of austenitic stainless steels is

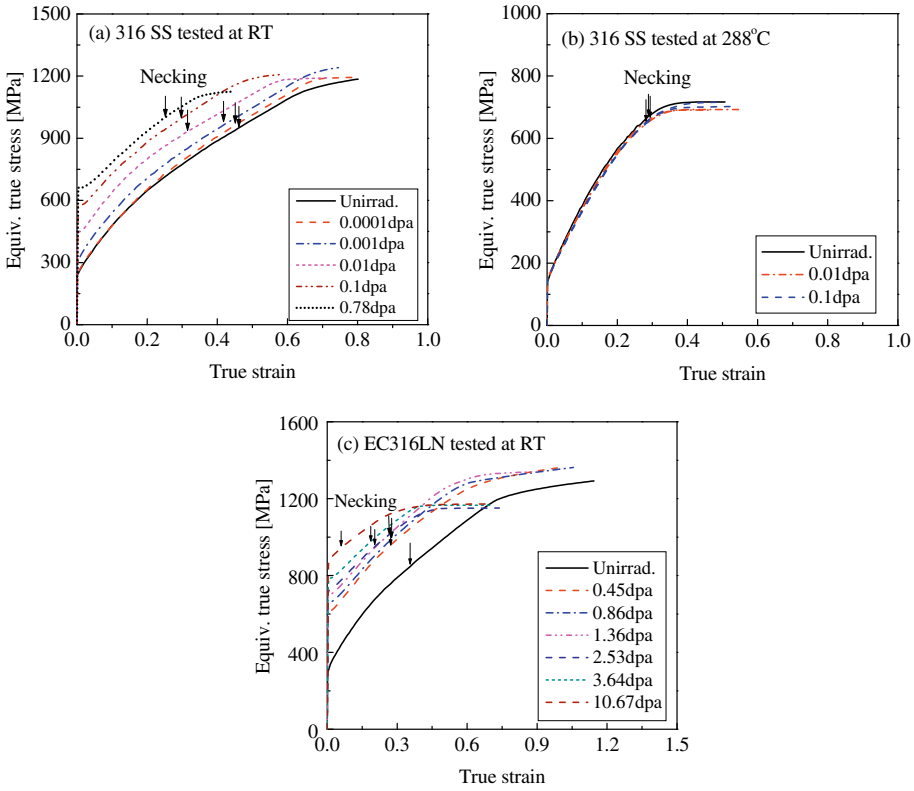

Fig. 5. Equivalent true stress–true strain curves for austenitic stainless steels after irradiation to various doses: (a) 316 SS at RT, (b) 316 SS at 288 °C, and (c) EC316LN at RT.

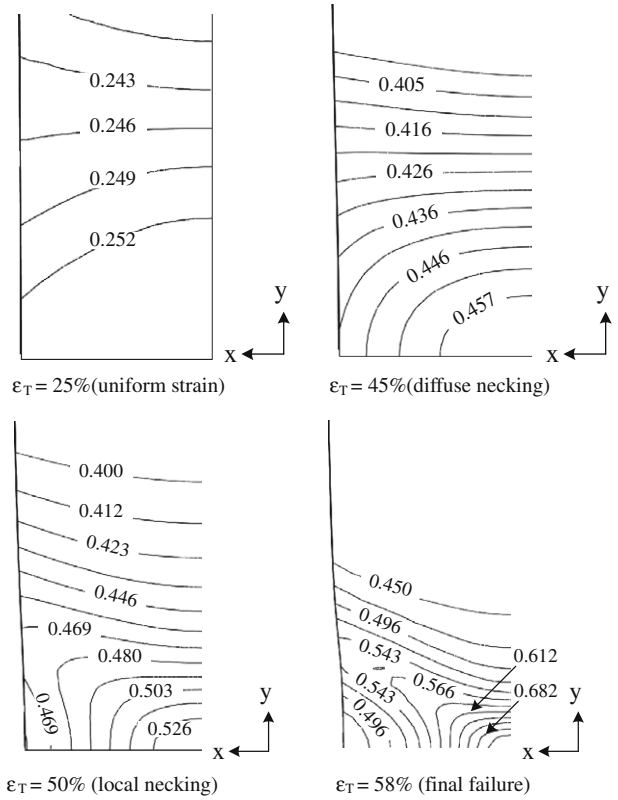

Fig. 6. Transition of necking mode with deformation: the change of maximum principal logarithmic strain contour at mid-section of 316SS specimen irradiated to 0.1 dpa.

planar slip at elevated temperatures above 200 °C. Since the strain hardening capability is exhausted early at 288 °C, the strain hardening during diffuse necking becomes negligible and thus diffuse necking is promptly transitioned into localized necking. This implies that the onset of localized necking is related to the exhausted strain hardening capability of materials as well as the change of stress state governed by specimen geometry.

The mechanistic reason for the reduced strain hardening rate in the localized necking is not well known for now. It is however speculated that the density of dislocation glides within the narrow localized bands might be much higher than in the prior uniform or diffused deformation, and therefore the annihilation of both the plasticity- and radiation-induced defects should be accelerated. This argument can explain the calculation result of reduced strain hardening rate as well as imply that the inelastic behavior of a material is an interactive property with geometrical factors.

4.2. Dose dependence of fracture properties

To investigate dose dependence of tensile fracture properties for austenitic stainless steels, the equivalent fracture stress, fracture strain, and tensile fracture energy were obtained from the equivalent true stress–true strain curves shown in the previous section. As discussed above, the true strains obtained for the localized necking are not accurate values for the localized necking area, and should be considered underestimated. In the discussions below the fracture parameters were evaluated both at the initiation of localized necking and at the point of final failure.

4.2.1. Equivalent fracture stress

Fig. 8 presents the equivalent fracture stresses for 316 SS and EC316LN SS as a function of irradiation dose (dpa), together with the yield stress (σ_{YS}) and plastic instability stress (σ_{PIS}) of each material. In Fig. 8, σ_{nL} is the equivalent fracture stress defined at initiation of localized necking and σ_{FE} is defined at the point of final failure. The variation in σ_{nL} with irradiation dose was almost the

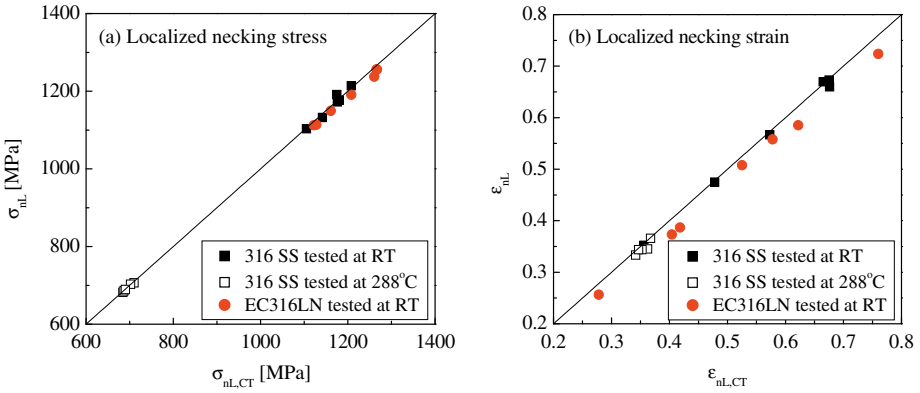

Fig. 7. Comparisons of (a) localized necking stresses and (b) localized necking strains determined by analytical criterion and strain contour change.

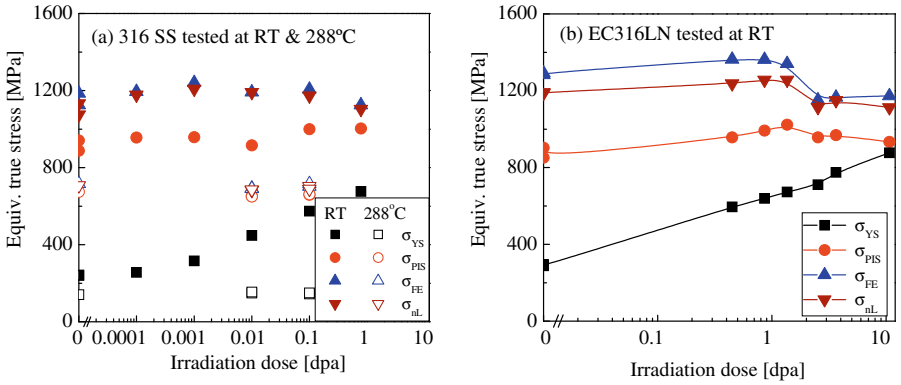

Fig. 8. Dose dependence of true stress parameters for austenitic stainless steels: (a) 316 SS and (b) EC316LN SS.

same as that of σ_{FE} regardless of tested material, even though the value of σ_{nL} was lower than that of σ_{FE}. For the 316 SS at RT, both σ_{nL} and σ_{FE} slightly increased at lower doses and then decreased with increasing irradiation dose. But their variations with dose were minor; the values of σ_{nL} and σ_{FE} at 0.78 dpa were nearly identical to those in nonirradiated condition, $\sigma_{nL,unir}$ and $\sigma_{FE,unir}$. For the EC316LN SS, the variations in σ_{nL} and σ_{FE} with irradiation dose were also negligible up to around 2 dpa, but the σ_{nL} and σ_{FE} abruptly dropped about 10% above 2 dpa. This result indicates that the equivalent fracture stress defined at either initiation of localized necking or final fracture is insensitive to irradiation dose up to, at least, 0.78 dpa in 316 SS and 10.7 dpa in EC316LN SS, except for the 10% drop of fracture stress around 2 dpa in EC316LN SS. The transition of equivalent fracture stress should be associated with a change in the irradiation damage and associated failure mechanism.

The EC316LN SS specimens were irradiated in the LANSCE accelerator as described in Section 2. In this case, it is known that helium and hydrogen gases are generated by spallation reactions [22]. At higher doses, in particular, the contents of the gas bubbles are considerable and they contribute to an extra strengthening in addition to the displacement damage. It was observed from the previous studies [3,4,22] that the yield stress and uniform elongation of EC316LN SS specimens irradiated in LANSCE accelerator tend to exceed the upper and lower bounds of the fission reactor data above 1 dpa, respectively. Maloy et al. [23] also observed a significant decrease in the uniform elongation above 3 dpa for 316 SS irradiated, which was different from the behavior observed for 316 SS irradiated by fission neutrons. It was explained that these behaviors are induced by large amount of retained gas generated by high energy proton and spallation neutron spectrum at higher dose. Therefore, it is concluded that the equivalent fracture stress of austenitic stainless steels is much less sensitive to irradiation dose unless the damage mechanism changes, although the yield stress considerably increases in the same dose range.

4.2.2. Fracture strain and tensile fracture energy

The variations in fracture strains defined at initiation of localized necking (ε_{nL}) and at final failure (ε_F) with irradiation dose are shown in Fig. 9 along with true uniform strain (ε_U). Overall dose dependence of ε_{nL} and ε_F was similar to that of ε_U for both materials, and the dose dependence of ε_{nL} was nearly the same as that of ε_F. For 316 SS at RT, the ε_{nL} and ε_F were relatively little changed over a lower dose below 0.01 dpa and then decreased exponentially with dose above 0.01 dpa. At the highest dose of 0.78 dpa the values of ε_{nL} and ε_F were still higher than 50% of the strain values before irradiation, $\varepsilon_{nL,unir}$ and $\varepsilon_{F,unir}$. The ε_{nL} and ε_F for EC316LN SS rapidly decreased with dose in the range 0–2 dpa and then decreased at lower rates after a small drop around 2 dpa. At a dose of 10.7 dpa, the values of ε_{nL} and ε_F were approximately 35% of $\varepsilon_{nL,unir}$ and 60% of $\varepsilon_{F,unir}$, respectively. Considering that the true uniform strain at 10.7 dpa was about 16% of that in nonirradiated condition, the reduction in fracture strain with irradiation dose was relatively small compared to the uniform strain. It is recognized from this result that the fracture strain of austenitic stainless steels is still high after irradiation exposure even if uniform ductility is considerably reduced. In Fig. 9, the dose dependence of fracture strain defined at initiation of localized necking was almost the same as that defined at final failure. The value of ε_{nL} was always lower than that of ε_F and the difference between ε_{nL} and ε_F was particularly significant in the EC316LN SS. This result should be mainly associated with the specimen geometry; the aspect ratio of specimen is 4.8 for

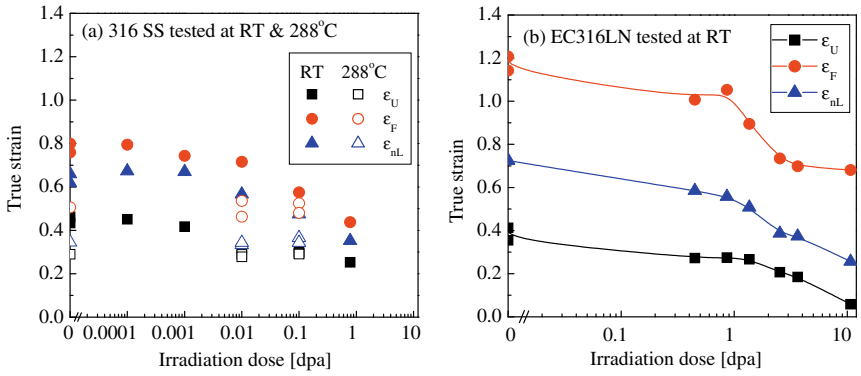

Fig. 9. Dose dependence of true strain parameters for austenitic stainless steels: (a) 316 SS and (b) EC316LN SS.

EC316LN SS and 6.0 for 316 SS. For a specimen with large aspect ratio, the tendency of localized necking is enhanced and necking band shrinks rapidly, whereas for a specimen with small aspect ratio the localized necking process after initiation is relatively slow due to the effect of stress in the thickness direction [19,20]. Thus, the amount of deformation from localized necking initiation to final failure is relatively higher and the difference between ε_{nL} and ε_F is more significant for the EC316LN SS when compared to the 316 SS.

The tensile fracture energy was obtained at both points of localized necking initiation (E_{nL}) and final failure (E_F) using Eq. (7) in the Part I [14]. As shown in Fig. 10, the variations in E_{nL} and E_F with dose for 316 SS at RT were negligible to 0.01 dpa, and then exponentially decreased with increasing dose to 0.78 dpa. For the EC316LN SS, the values of E_{nL} and E_F apparently decreased as irradiation dose increased to around 2 dpa and then they were slightly dropped and slowly saturated above 2 dpa. The values of E_{nL} and E_F at 10.7 dpa were still higher than, respectively, 43% and 67% of the energies obtained in unirradiated condition. This indicates that the resistance to tensile fracture of austenitic stainless steels considerably decreased, but a significant resistance to fracture still remained after irradiation to 0.78 for 316 SS and 10.7 dpa for the EC316LN SS. Such dose dependence of tensile fracture energy agrees well with that of fracture toughness for austenitic stainless steels [23].

It is known that the yield stress for austenitic stainless steels increases rapidly with irradiation dose up to about 0.1 dpa in the low temperature irradiations and that the increasing rate slows with further increase in dose until the hardening reaches a saturation value in the dose range of 1–3 dpa [2]. Microstructural observation revealed that such a dose dependence was attributed to the increase in the density of irradiation-induced defects, i.e., black spot damage and Frank loops, which saturated at doses of about 0.1 and 1 dpa, respectively [24]. Thus the considerable decrease in fracture strain and tensile fracture energy at lower doses below 2 dpa and the saturation above this dose are simply explained by the change in the density of such irradiation-induced defects. Also, the small drops of fracture strain and tensile fracture energy around 2 dpa are believed to be related to the additional irradiation damage mechanism, e.g., helium and hydrogen gas generation, as discussed previous section.

4.2.3. Influence of material and test temperature

To understand an influence of material on dose dependence of fracture properties for austenitic stainless steels, the values of σ_{nL}, ε_{nL}, and E_{nL} for 316 SS and EC316LN SS were compared. Since the tensile fracture properties defined at the initiation of localized necking were more reliable than those defined at final failure, here comparisons were made using these parameters. The fracture properties for both materials were nearly the same at nonirradiated condition. However, the properties for 316 SS were more drastically changed with dose compared to EC316LN SS, so that the difference between the 316 SS and the EC316LN became more profound at higher doses although the differences in the σ_{PIS} and ε_U values of the two materials were small over the dose range examined. In particular, the difference between materials was apparent at ε_{nL} and E_{nL}; the tensile fracture properties for the EC316LN SS were less sensitive to irradiation dose than those for the 316 SS. This should be associated with different strain hardening capability between the two stainless steels. It is believed that the addition of nitrogen in the EC316LN SS has decreased its stacking fault energy (SFE), and thereby increased its tendency for mechanical twinning [11]. This mechanical twinning can increase strain hardening capability and delay deformation localization and localized necking

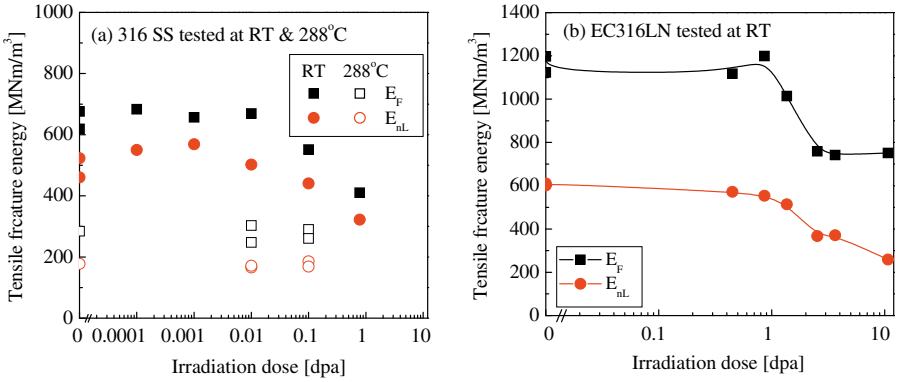

Fig. 10. Dose dependence of tensile fracture energy for austenitic stainless steels (a) 316 SS and (b) EC316LN SS.

initiation in austenitic stainless steels [25]. Therefore, the deformation localization and the reduction of strain hardening capability by irradiation are more delayed in the EC316LN SS, which results in higher fracture strain and energy in this steel. Such a difference between the two steels is more significant at high doses where the deformation localization is much enhanced by irradiation.

The effect of test temperature on the fracture properties of 316 SS is shown in Figs. 8–10. Compared to the properties tested at RT, the variations in equivalent fracture stress, fracture strain, and tensile fracture energy with dose to 0.1 dpa were negligible for the specimens tested at 288 °C. This is mainly attributed to the high irradiation temperature, about 350 °C, for specimens tested at 288 °C, in contrast to the specimens tested at RT after irradiation in the temperature range 60–100 °C. This shows that the irradiation damage for specimens tested at 288 °C was negligible due to thermal annealing during irradiation. This is evidenced by no obvious increase in yield stress after irradiation to 0.1 dpa (see Fig. 8). It is confirmed that the strain hardening rate and fracture properties for austenitic stainless steels are not obviously affected by irradiation exposure to 0.1 dpa if they are irradiated and loaded around 300 °C.

4.3. Comment on the results of approximation model [10]

In the present study it was shown that the high strain hardening rate in the austenitic stainless steels after significant irradiation was still retained beyond the onset of necking and the hardening rate was nearly independent of dose until the localized necking initiated. Also, it was observed that the fracture stress is little dependent on irradiation dose. Although the fracture strain was more sensitive to irradiation dose, it was retained at a few tens of percent after irradiation exposure to high doses. These results were based on the equivalent true stress and true strain relation of material, which involves multi-axial stress components at the neck during unstable deformation. A comparison of these simulation results with the results of earlier studies [7,9,11] confirms that the two different methods, the present multi-axial finite element analysis and an analytical linear approximation model can produce consistent results for the dose dependences of unstable deformation and fracture parameters. The linear approximation model assumes a linear strain hardening during unstable deformation and considers nominal (or axial) true stress–true strain relation. Fig. 11 compares the fracture stresses obtained from the finite element simulation (equivalent and nominal or components) those from the linear approximation model (nominal component). This comparison indicates that the nominal fracture stress from this simulation is close to the result of the linear approximation model (note that the small difference may originate from the non-detailed treatment of final localized necking in both methods), while, as expected, the equivalent fracture stress is lower than the nominal components. It is therefore believed that the fracture stress data from the linear approximation model are accurate enough to use in evaluation of hardened materials such as irradiated materials, in which unstable deformation is dominant and direct strain measurement can be costly. For an application, it is worth remembering that the linear hardening model, which is for the true stress in the axial direction, can describe deformation up to the onset of localized necking, even though the two transverse stress components during necking cannot be known by the model.

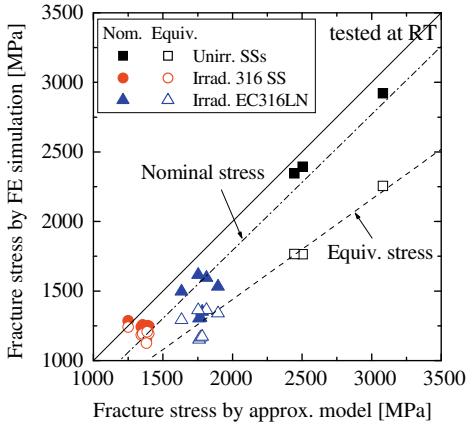

Fig. 11. Comparison of fracture stresses obtained from finite element simulation and approximation model.

5. Conclusions

This study investigated the dose dependence of strain hardening behavior and tensile fracture properties for austenitic stainless steels based on the equivalent true stress–true strain curve data for 316 SS and EC316LN SS irradiated to various doses. The full equivalent true stress–true strain curves were determined using iterative finite element simulations. The conclusions from the analysis results are:

(1) Before the localized necking the strain hardening rate during unstable deformation was retained at a high level, which was similar to that in the end of uniform deformation. The strain hardening behavior during necking was nearly independent of dose.
(2) The variation in equivalent fracture stress with dose was negligible for the austenitic stainless steels unless irradiation damage mechanism changed.
(3) The tensile fracture strain and fracture energy of austenitic stainless steels decreased with dose in the low dose range <2 dpa and at higher doses they approached lowered saturation values, which were still significantly high for highly irradiated materials.
(4) Tensile fracture properties for EC316LN SS were less sensitive to the irradiation dose than those for 316 SS although their uniform tensile properties showed similar dose dependences.
(5) A comparison with the results from the present multi-axial finite element analysis confirmed that the linear approximation model for unstable deformation can reasonably well describe the dose dependences of tensile fracture properties.

Acknowledgements

This study was sponsored by the Nuclear Research and Development Program of the National Research Foundation (NRF) under the Korean Ministry of Education, Science and Technology (MEST) (Grant Code: 2009-0078103). The experimental data used in this study was from earlier studies at Oak Ridge National Laboratory sponsored by the US Department of Energy, Offices of Fusion Energy Sciences and Basic Energy Science, under Contract DE-AC05-00OR22725 with UT-Battelle, LLC. The authors express special thanks to Drs. John G. Merkle and C.S. Shin for their technical reviews and thoughtful comments.

References

[1] Y. Dai, G.W. Egeland, B. Long, J. Nucl. Mater. 377 (2008) 109.
[2] J.E. Pawel, A.F. Rowcliffe, G.E. Licas, S.J. Zinkle, J. Nucl. Mater. 239 (1996) 126.
[3] K. Farrell, T.S. Byun, J. Nucl. Mater. 296 (2001) 129.
[4] T.S. Byun, K. Farrell, E.H. Lee, L.K. Mansur, S.A. Maloy, M.R. James, W.R. Johnson, J. Nucl. Mater. 303 (2002) 34.
[5] S. Saito, K. Kikuchi, K. Usami, A. Ishikawa, Y. Nishino, M. Kawai, Y. Dai, J. Nucl. Mater. 343 (2005) 253.

[6] K. Farrell, T.S. Byun, Oak Ridge National Laboratory Report SNS/TR-211, January 2001.
[7] T.S. Byun, K. Farrell, E.H. Lee, J.D. Hunn, L.K. Mansur, J. Nucl. Mater. 298 (2001) 269.
[8] T.S. Byun, K. Farrell, Acta Mater. 52 (2004) 1597.
[9] T.S. Byun, J. Nucl. Mater. 361 (2007) 239.
[10] T.S. Byun, K. Farrell, M. Li, Acta Mater. 56 (2008) 1056.
[11] T.S. Byun, K. Farrell, M. Li, Acta Mater. 56 (2008) 1044.
[12] T.S. Byun, N. Hashimoto, K. Farrell, J. Nucl. Mater. 351 (2006) 303.
[13] T.S. Byun, N. Hashimoto, Nucl. Eng. Technol. 38 (2006) 619.
[14] J.W. Kim, T.S. Byun, J. Nucl. Mater. 396 (2010) 1.
[15] K. Farrell, T.S. Byun, N. Hashimoto, Oak Ridge National Laboratory Report SNS/TM-2003/63, 2003.
[16] Hibbitt, Karlson, and Sorensen Inc., ABAQUS Ver. 6.5 User's Manual, 2005.
[17] Y. Bao, Eng. Frac. Mech. 72 (2005) 502.
[18] P. Koc, B. Stok, Compos. Mater. Sci. 31 (2004) 155.
[19] V. Tvergaard, Compos. Meth. Appl. Mech. Eng. 103 (1993) 273.
[20] K. Ikeda, S. Okazawa, K. Terada, H. Noguchi, T. Usami, Int. J. Eng. Sci. 39 (2001) 1913.
[21] G.E. Dieter, Mechanical Metallurgy, SI Metric Ed., McGraw-Hill, Inc., 1988.
[22] J.D. Hunn, E.H. Lee, T.S. Byun, L.K. Manusr, J. Nucl. Mater. 282 (2000) 131.
[23] S.A. Maly, M.R. James, G. Willcutt, W.F. Sommer, M. Sokolov, L.L. Snead, M.L. Hamilton, F. Garner, J. Nucl. Mater. 296 (2001) 119.
[24] S.J. Zinkle, P.J. Maziasz, R.E. Stoller, J. Nucl. Mater. 206 (1993) 266.
[25] T.S. Byun, N. Hashimoto, K. Farrell, Acta Mater. 52 (2004) 3889.